

A Flexible Generalized Low-Rank Regularizer for Tensor RPCA

Anonymous submission

Abstract

A plethora of previous Tensor Robust Principal Component Analysis (TRPCA) methods utilize Tensor Nuclear Norm (TNN) minimization for recovering the low-rank tensor from corrupted observation. However, minimizing the TNN faces some limitations. For example, TNN penalizes each singular value of the low-rank tensor uniformly, leading to a sub-optimal solution. This is because larger singular values typically represent more significant data features and should be penalized less. In this paper, we devise a **flexible generalized** low-rank regularizer that adaptively assigns varying penalties based on the magnitude of the singular values. Additionally, considering the local smoothness property inherent in some tensor data, we apply the regularizer to capture low-rankness in the gradient domain. Our models show two characteristics with 1) **generalization**, i.e., our models include many existing popular works. 2) **flexibility**, i.e., our regularizer is not merely a combination of many discrete works but achieves transformation by adjusting a continuous shape parameter. Moreover, we develop efficient algorithm frameworks via the Alternating Direction Method of Multipliers (ADMM) to implement our models. Experimental results on recovery tasks validate the superiority of our models.

Introduction

Tensor data are ubiquitous: many real-world data are often inherently multidimensional, with information stored in multi-way arrays known as tensors, e.g., images, videos, bioinformatics, network flow data, etc. In recent years, significant advancements across various interdisciplinary domains have been made in tensor analysis, such as machine learning (Wen, Chen, and Chen 2024; Phothilimthana et al. 2024), data mining (Zhang et al. 2023a; Huang et al. 2024), and computer vision (Zhao et al. 2024; Liu et al. 2024a). However, due to the limitations of signal acquisition equipment, such as sensor sensitivity, photon effects, and calibration errors, tensor data collected in the real world often exhibit significant corruption. Consequently, tensor denoising has become a crucial task in tensor analysis.

In this paper, we focus on the Tensor Robust Principal Component Analysis (TRPCA) problem. Consider a corrupted tensor data $\mathcal{M} \in \mathbb{R}^{d_1 \times d_2 \times d_3}$, TRPCA seeks to recover the underlying low-rank tensor \mathcal{L} and sparse tensor \mathcal{E} from their sum \mathcal{M} (see Fig. 1 for an intuitive illustration)

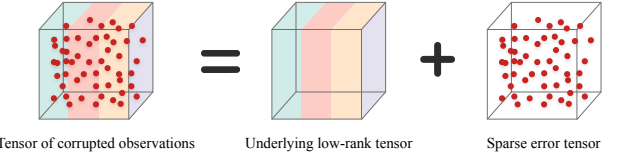


Figure 1: An illustration of TRPCA, which aims to recover the low-rank and sparse components from the observation.

and solves the following problem

$$\min_{\mathcal{L}, \mathcal{E}} \text{rank}(\mathcal{L}) + \lambda \|\mathcal{E}\|_1 \quad \text{s.t. } \mathcal{M} = \mathcal{L} + \mathcal{E}, \quad (1)$$

where $\lambda > 0$ is a regularization parameter. $\text{rank}(\mathcal{L})$ denotes the rank of clean tensor \mathcal{L} and $\|\mathcal{E}\|_1$ is ℓ_1 -norm (sum of the absolute values of all the entries) of the sparse tensor \mathcal{E} . One of the primary challenges in extending RPCA to tensor data is defining the tensor rank, which is more sophisticated than the matrix rank. Many classical definitions of tensor rank such as the CANDECOMP/PARAFAC (CP) rank (Hitchcock 1927), the Tucker rank (Kolda and Bader 2009), and the tensor tubal rank (Kilmer and Martin 2011).

The CP rank is defined as the smallest number of rank-one tensors that sum to the given tensor (Hitchcock 1927). Despite its utility, applying CP rank to the TRPCA method is challenging since computing the exact CP rank is known to be an NP-hard problem. The Tucker rank of an n -way tensor \mathcal{X} is defined as an n -dimensional vector, where the i -th entry is the rank of the mode- i matricization $\mathcal{X}_{(i)}$. Mathematically, the Tucker rank is expressed as $\text{rank}_{tc}(\mathcal{X}) = [\text{rank}(\mathcal{X}^{\{1\}}), \dots, \text{rank}(\mathcal{X}^{\{k\}})]$. The Sum of Nuclear Norms (SNN) can be viewed as a convex surrogate for the Tucker rank, which is defined as $\sum_i \|\mathcal{X}_*^{\{i\}}\|$. Nonetheless, computing the Tucker rank remains complex, particularly for large-scale tensors, due to the non-convex nature of the optimization algorithm (Huang et al. 2015). The aforementioned issues have prompted tensor tubal rank derived from the tensor Singular Value Decomposition (t-SVD) as an alternative to the tensor rank (Kilmer and Martin 2011). Based on tensor tubal rank, a new tensor nuclear norm has been proposed and applied within the TRPCA framework (Lu et al. 2020)

$$\min_{\mathcal{L}, \mathcal{E}} \|\mathcal{L}\|_* + \lambda \|\mathcal{E}\|_1 \quad \text{s.t. } \mathcal{M} = \mathcal{L} + \mathcal{E}, \quad (2)$$

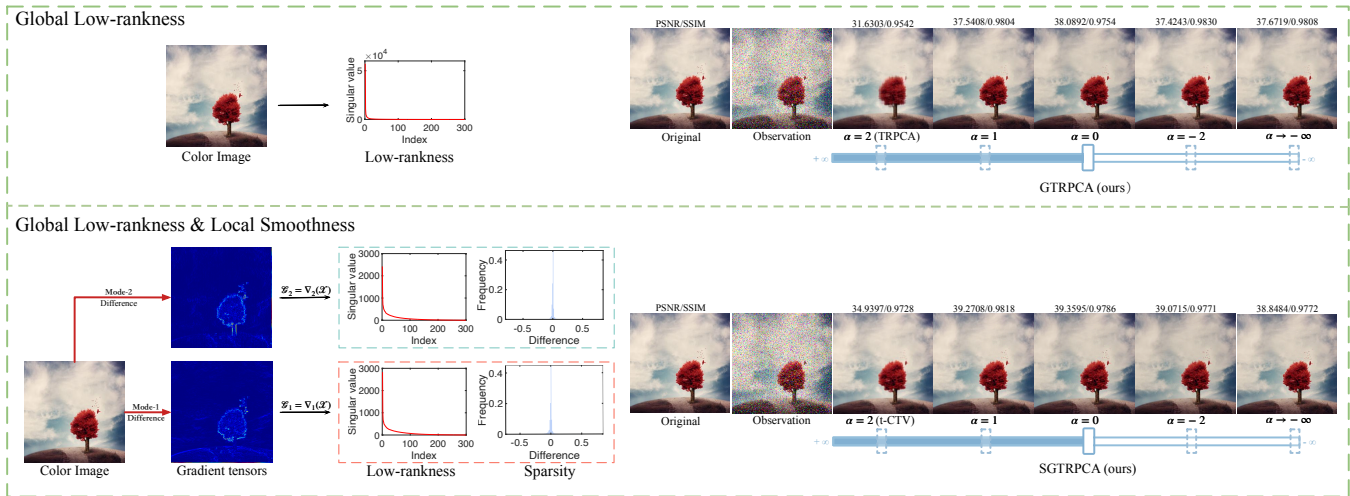


Figure 2: Take a color image sample from "ZJU" database as an example. The two frames illustrate that under different structure priors of color images, the recovery performances of our proposed GTRPCA and SGTRPCA with different shape parameter α .

where $\|\cdot\|_*$ denotes the tensor nuclear norm (TNN). Moreover, the recent works (Kilmer et al. 2021) have proved the optimal representation and compression theories of t-SVD, making model (2) significantly more notable in characterizing the intrinsic low-rank structures of tensors. As a result, the model (2) under t-SVD has garnered considerable interest recently (Hou et al. 2024; Liu et al. 2024c; Qin et al. 2024).

Despite the impressive performance of TRPCA, it still exhibits several limitations. Specifically, when minimizing the TNN, TRPCA employs tensor singular value thresholding, which uniformly shrinks all singular values. In real-world applications, singular values often carry distinct physical meanings, with prior knowledge suggesting that larger singular values are typically associated with more significant information. The uniform shrinkage approach of TRPCA fails to account for these differences among singular values, potentially leading to suboptimal results.

Many advanced methodologies for improving TRPCA have been proposed to alleviate such limitations. (Gao et al. 2020) proposed the Enhanced TRPCA (ETRPCA) method, which utilizes a weighted tensor nuclear norm with the Schatten p -norm to assign different weights to singular values. However, ETRPCA requires predefined, fixed weights manually set in advance. (Jiang et al. 2020) put forward the Partial Sum of the Tubal Nuclear Norm (PSTNN) as a surrogate of TNN. PSTNN only shrinks small singular values and keeps large singular values fixed. This approach implicitly assumes that the large singular values are irrelevant to the content of the tensor. To adaptively learn weights to penalize distinct singular values, (Liu et al. 2024b) devised a novel Tensor Improved Huber Norm (TIHN) to shrink all singular values exactly and adaptively. Interestingly, it is apparent that these norm constraints are essentially equivalent to imposing sparse constraints on singular values through sparse norms. The previously mentioned methods primarily enhance constraints on the low-rank component while ne-

glecting improvements to the constraint on the sparse component. Very recently, several strategies have been proposed to refine the sparse constraint. (Wang et al. 2023b) proposed a Double Auto-weighted TRPCA (DATRPCA) which takes into account the significance of different singular values of the low-rank tensor and entries of the sparse tensor simultaneously. (Zhang et al. 2023b) introduced two generalized regularizers encompassing a variety of popular functions as better surrogates of TNN and Tensor ℓ_1 -norm (TL1N). In addition, (Yan and Guo 2024) developed a new TRPCA model based on dual ℓ_p -norm sparse constraints (weighted ℓ_p -norm on low-rank component and ℓ_p -norm on sparse component).

Obviously, such methods for improving both the low-rank and sparse components of TRPCA have much in common. They generally enhance the performance of TRPCA by penalizing different singular values of the low-rank tensor and the distinct entries of the sparse tensor. In this paper, we design a novel low-rank regularizer to adaptively assign smaller penalties to larger singular values with **1) generalization**, i.e., by introducing a continuous-valued parameter, we have shown that our framework can be tuned to several existing models with specific values of α including the original TRPCA (Lu et al. 2020) model, and can be annealed to the original TRPCA (Lu et al. 2020); **2) flexibility**, i.e, except for the existing works, α can be adjusted to wider unexplored models to improve performance since α can theoretically take on an infinite range of values. Additionally, we extend the regularizer to the sparse component and propose a novel Generalized TRPCA model called GTRPCA.

Besides the global low-rankness prior, the local smoothness prior represented by total variation (TV) is also generally applied in tensor recovery fields (Ko et al. 2020; Qiu et al. 2021). This prior represents a general structural property of a practical visual tensor. Adjacent pixels along a tensor mode tend to change continuously, indicating a type of information similarity at a relatively local scale. Many previous works have incorporated the local smoothness prior

into the traditional global low-rankness prior model and achieved better performance (Peng et al. 2020, 2022). However, these studies encoded the two priors as the sum of two independent regularization terms in the recovery model and adjusted the corresponding regularization parameters to enhance model performance. However, because these two priors are often interdependent, establishing general guidelines for fine-tuning the two trade-off parameters in real-world scenarios is challenging. This consistently presents a considerable challenge in formulating a comprehensive rule for precisely tuning this balancing parameter in practical applications. Moreover, the theoretical guarantee for exact recovery remains unproven for the related methods.

Given the circumstances above, (Wang et al. 2023a) proposed the tensor Correlated Total Variation (t-CTV) norm which integrates the two priors into a single regularization term, eliminating the need for tuning separate parameters. Additionally, this work provided theoretical guarantees for the exact recovery of similar tensor methods that jointly model both priors. Analogously, the integration regularization term was also based on TNN in the gradient domain. Consequently, (Huang et al. 2024) proposed a reweighted regularizer based on ℓ_p norm as a surrogate for t-CTV term. In this paper, we extend our proposed regularizer to the gradient domain and propose a novel tensor-correlated flexible generalized joint prior (t-FGJP) regularizer.

Our main contributions can be delineated as follows:

- We propose a generalized and flexible low-rank regularizer that accounts for the varying importance of different singular values in low-rank tensors to preserve critical information. By introducing a continuous parameter α , our model can equivalently represent several existing models with specific values of α and can be adjusted to encompass a broader range of models. Additionally, we extend the regularizer to the sparse component and propose a novel generalized TRPCA model called GTRPCA.
- Moreover, taking into account the local smoothness prior, our regularizer is available in the gradient domain (t-FGJP) to capture the low-rank structure of the gradient tensors with different directions. The t-FGJP regularizer also maintains the flexibility of discriminatively controlling different singular values of the gradient tensors and is applied to the proposed smooth GTRPCA (SGTRPCA) model.
- We design ADMM-based algorithmic frameworks tailored for each of the aforementioned models. Experimental results demonstrate that our models exhibit strong generalization capabilities and outperform existing TRPCA models.

Notations and preliminaries

To begin with, we introduce some essential notations and definitions utilized throughout the paper. We use lowercase letters, boldface lowercase letters, and boldface uppercase letters to denote scalars, e.g., x , vectors, e.g., \mathbf{x} , and matrices, e.g., \mathbf{X} , respectively. Tensors are presented by bold calligraphic letters, e.g., \mathcal{X} . For a 3-order tensor

Notation	Description
$\mathcal{X}, \mathbf{X}, \mathbf{x}, x$	tensor, matrix, vector, scalar
$\mathcal{X} \in \mathbb{R}^{d_1 \times d_2 \times d_3}$	observed tensor
\mathcal{X}_{ijk} or $\mathcal{X}(i, j, k)$	(i, j, k) -th entry of \mathcal{X}
$\mathcal{X}(i, :, :)$	i -th horizontal slice of \mathcal{X}
$\mathcal{X}(:, j, :)$	j -th lateral slice of \mathcal{X}
$\mathbf{X}^{(k)}$ or $\mathcal{X}(:, :, k)$	k -th frontal slice of \mathcal{X}
DFT	Discrete Fourier Transform
$\tilde{\mathcal{X}} \in \mathbb{C}^{d_1 \times d_2 \times d_3}$	DFT of \mathcal{X} along the 3-rd dimension
$\tilde{\mathbf{X}}^{(k)} \in \mathbb{C}^{d_1 \times d_2}$	k -th frontal slice of $\tilde{\mathcal{X}}$
$\ \mathcal{X}\ _{\ast}$	Tensor Nuclear Norm (TNN)
$\ \mathcal{X}\ _1$	Tensor ℓ_1 Norm (TL1N)
$\ \mathcal{X}\ _F$	Tensor Frobenius Norm
$\ \mathcal{X}\ _\infty$	Tensor infinity Norm

Table 1: Key notations used in this paper.

$\mathcal{X} \in \mathbb{R}^{d_1 \times d_2 \times d_3}$, we denote \mathcal{X}_{ijk} as its (i, j, k) -th entry, $\mathcal{X}(i, :, :)$ as its horizontal slice, $\mathcal{X}(:, j, :)$ as its lateral slice, $\mathcal{X}(:, :, k)$ as its frontal slice, respectively. For convenience, the frontal slice $\mathcal{X}(:, :, k)$ is often denoted as $\mathbf{X}^{(k)}$. The tensor ℓ_1 norm (TL1N), tensor Frobenius norm and tensor infinity norm of \mathcal{X} are defined by $\|\mathcal{X}\|_1 = |\mathcal{X}_{ijk}|$, $\|\mathcal{X}\|_F = \sqrt{\sum_{ijk} |\mathcal{X}_{ijk}|^2}$ and $\|\mathcal{X}\|_\infty = \max_{ijk} |\mathcal{X}_{ijk}|$, respectively. The conjugate transpose of $\tilde{\mathcal{X}} \in \mathbb{C}^{d_1 \times d_2 \times d_3}$ is defined as $\tilde{\mathcal{X}}^T \in \mathbb{C}^{d_2 \times d_1 \times d_3}$, its first frontal slice equals $(\tilde{\mathbf{X}}^{(1)})^T$ while the rest of the frontal slices equal to $(\tilde{\mathbf{X}}^{(d_3+2-k)})^T, k = 2, 3, \dots, d_3$. Table 1 provides a summary of the key notations and their descriptions used in the paper.

Definition 1. (t-product) (Kilmer et al. 2013) The t-product $\mathcal{A} * \mathcal{B}$ of any two 3-order tensor $\mathcal{A} \in \mathbb{R}^{d_1 \times d_2 \times d_3}$ and $\mathcal{B} \in \mathbb{R}^{d_2 \times d_4 \times d_3}$ is defined to be a tensor of size $d_1 \times d_4 \times d_3$

$$\mathcal{A} * \mathcal{B} = \text{fold}(\text{bcirc}(\mathcal{A}) \cdot \text{unfold}(\mathcal{B})),$$

where we define the operator $\text{unfold}(\cdot)$ as $\text{unfold}(\mathcal{B}) = [\mathbf{B}^{(1)T} \mathbf{B}^{(2)T} \dots \mathbf{B}^{(d_3)T}]^T$ and its inverse operator $\text{fold}(\cdot)$ as $\text{fold}(\text{unfold}(\mathcal{B})) = \mathcal{B}$. The block circulant matrix of \mathcal{A} is defined as

$$\text{bcirc}(\mathcal{A}) = \begin{bmatrix} \mathbf{A}^{(1)} & \mathbf{A}^{(d_3)} & \dots & \mathbf{A}^{(2)} \\ \mathbf{A}^{(2)} & \mathbf{A}^{(1)} & \dots & \mathbf{A}^{(3)} \\ \vdots & \vdots & \ddots & \vdots \\ \mathbf{A}^{(d_3)} & \mathbf{A}^{(d_3-1)} & \dots & \mathbf{A}^{(1)} \end{bmatrix} \in \mathbb{R}^{d_1 d_3 \times d_2 d_3},$$

In fact, the t-product $\mathcal{X} = \mathcal{A} * \mathcal{B}$ can be computed efficiently using the fft . Specifically, let $\bar{\mathcal{A}} = \text{fft}(\mathcal{A}, [], 3)$ and $\bar{\mathcal{B}} = \text{fft}(\mathcal{B}, [], 3)$. We can calculate the k -th frontal slice of $\bar{\mathcal{Z}}$ by $\bar{\mathcal{Z}}^{(k)} = \bar{\mathcal{A}}^{(k)} \bar{\mathcal{B}}^{(k)}$ and obtain $\mathcal{Z} = \text{ifft}(\bar{\mathcal{Z}}, [], 3)$.

Based on these definitions above, the factorization strategy (t-SVD) for the 3-order tensors is as follows.

Definition 2. (T-SVD) (Kilmer and Martin 2011) For a tensor $\mathcal{X} \in \mathbb{R}^{d_1 \times d_2 \times d_3}$, it can be factorized by t-SVD as

$$\mathcal{X} = \mathcal{U} * \mathcal{S} * \mathcal{V}^T, \quad (3)$$

where $\mathcal{U} \in \mathbb{R}^{d_1 \times d_1 \times d_3}$, $\mathcal{V} \in \mathbb{R}^{d_2 \times d_2 \times d_3}$ are orthogonal tensors, i.e., $\mathcal{U} * \mathcal{U}^T = \mathcal{U}^T * \mathcal{U} = \mathcal{V} * \mathcal{V}^T = \mathcal{V}^T * \mathcal{V} = \mathcal{I}$,

and $\mathcal{S} \in \mathbb{R}^{d_1 \times d_2 \times d_3}$ is an f -diagonal tensor, i.e., its frontal slices are the diagonal matrices.

Definition 3. (Tensor Nuclear Norm, TNN) (Lu et al. 2020) For $\mathcal{X} \in \mathbb{R}^{d_1 \times d_2 \times d_3}$ and $d = \min(d_1, d_2)$, the Tensor Nuclear Norm of \mathcal{X} is defined as

$$\|\mathcal{X}\|_* = \frac{1}{d_3} \sum_{k=1}^{d_3} \sum_{i=1}^d \sigma_i(\bar{\mathbf{X}}^{(k)}), \quad (4)$$

where $\bar{\mathcal{X}}$ is the result by applying DFT on \mathcal{X} along the third dimension, $\bar{\mathbf{X}}^{(k)}$ is the k -th slice of $\bar{\mathcal{X}}$, $\sigma_i(\bar{\mathbf{X}}^{(k)})$ is the i -th singular value of $\bar{\mathbf{X}}^{(k)}$, and $d = \min(d_1, d_2)$.

The proposed method

In this part, we first introduce the proposed flexible generalized low-rank regularizer and our proposed GTRPCA model. Secondly, we devise an efficient optimization algorithm to implement GTRPCA. Except for global low-rankness prior, many tensor data also exhibit local smoothness structure. Fortunately, our low-rank regularization term can be leveraged to capture the low-rank structure in the gradient domain. Based on this, we further devise a regularizer and propose the smooth GTRPCA (SGTRPCA) model.

Flexible Generalized TNN

According to Definition 3, the original TNN uniformly shrinks each singular value of the low-rank tensor \mathcal{L} when minimizing the tensor nuclear norm. However, research has shown that larger singular values typically represent the most significant information in the data. Therefore, it is essential to apply less shrinkage to the larger singular values while increasing the shrinkage for the smaller ones to better preserve critical information. Conversely, taking into account the current enhancements to TNN, we introduce a flexible generalized tensor nuclear norm (FGTNN) defined below. Notably, our model does not merely aggregate discrete models. Rather, it generalizes into a broader framework through a continuous parameter α . This grants our model flexibility on top of its generalization.

Definition 4. (FGTNN) For a tensor $\mathcal{X} \in \mathbb{R}^{d_1 \times d_2 \times d_3}$, $d = \min(d_1, d_2)$, the Flexible Generalized Tensor Nuclear Norm (FGTNN) is defined as follows

$$\|\mathcal{X}\|_{G,*} = \frac{1}{d_3} \sum_{k=1}^{d_3} \sum_{i=1}^d g\left(\sigma_i(\bar{\mathbf{X}}^{(k)})\right), \quad (5)$$

where $d = \min\{d_1, d_2\}$, $g(\cdot)$ follows the below definition that we are about to introduce.

The simplest form of the proposed generalized loss $g(x)$ is:

$$g(x) = 2c \cdot \frac{|\alpha - 2|}{\alpha} \left(\left(\frac{|x|/c}{|\alpha - 2|} + 1 \right)^{\alpha/2} - 1 \right), \quad (6)$$

where $\alpha \in \mathbb{R}$ is a continuous-valued parameter that controls the penalty of the loss and $c > 0$ is a constant. Obviously, a main superiority of our loss is that it is a superset of many

Value of α	Formula ($c > 0$)
$\alpha = 2$	$ x $
$\alpha = 1$	$2c \left(\sqrt{ x /c + 1} - 1 \right)$
$\alpha = 0$	$2c \ln \left(\frac{1}{2} x /c + 1 \right)$
$\alpha = -2$	$2c \frac{2 x /c}{ x /c + 4}$
$\alpha \rightarrow -\infty$	$2c(1 - \exp(- x /2c))$
otherwise	$2c \frac{ \alpha - 2 }{\alpha} \left(\left(\frac{ x /c}{ \alpha - 2 } + 1 \right)^{\alpha/2} - 1 \right)$

Table 2: Formulas of the proposed generalized loss $g(x)$.

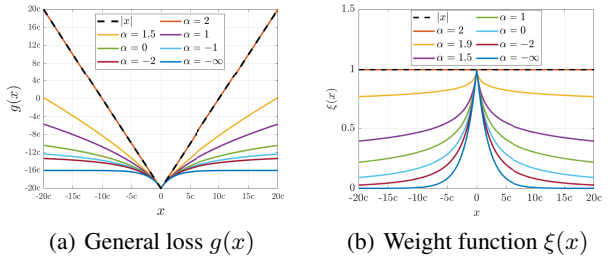


Figure 3: Our general loss $g(x)$ and the corresponding weight function $\xi(x)$.

existing functions with several values of α and its removable singularities at $\alpha = 0$ and $\alpha = 2$ and its limit at $\alpha = -\infty$. With this analysis, Table 2 presents our generalized loss with some special cases.

Remark 1. Fig. 3 intuitively presents the characteristics of our generalized loss $g(x)$. Overall, it is observed that $g(x)$ increases slower than $|x|$ for all values of α , which means less shrunk to large singular values, which fundamentally represents the essence of our improvements. More importantly, α appears to be related to the shape of $g(x)$. When $\alpha \rightarrow -\infty$, $g(x)$ follows an approximately exponential form; When $\alpha = 0$, $g(x)$ takes a logarithmic form; When $\alpha = 2$, $g(x)$ reduces to $|x|$; And in the other case of α , $g(x)$ is represented in a power form. The generation and flexibility characters enable our loss to better adapt to various scenarios. Moreover, parameter c regulates the intensity of the shrinkage. For example, with α and x held constant, larger c corresponds to a smaller magnitude of the shrinkage.

To best of our knowledge, this is the first generalized function designed to constrain the singular values. We have shown that many previous methods for improving TNN are special cases of FGTNN with a specific value of α .

Analogously, the proposed Generalized function can be used to characterize the significance of the different entries of the sparse tensor \mathcal{E} , thus we define the flexible generalized tensor L1 norm (FGTL1N).

Definition 5. (FGTL1N) For a tensor $\mathcal{X} \in \mathbb{R}^{d_1 \times d_2 \times d_3}$, the Flexible Generalized Tensor L1 Norm (FGTL1N) is defined

as follows:

$$\|\mathcal{X}\|_{G,1} = \sum_{i=1}^{d_1} \sum_{j=1}^{d_2} \sum_{k=1}^{d_3} g(|\mathcal{X}_{ijk}|), \quad (7)$$

Flexible Generalized TRPCA

By incorporating both FGTTNN and FGTL1N into TRPCA framework, we have the following Generalized TRPCA model

$$\min_{\mathcal{L}, \mathcal{E} \in \mathbb{R}^{d_1 \times d_2 \times d_3}} \|\mathcal{L}\|_{G,*} + \lambda \|\mathcal{E}\|_{G,1} \text{ s.t. } \mathcal{M} = \mathcal{L} + \mathcal{E}. \quad (8)$$

Note that our generalized loss includes a series of specific functions that are nonlinear and complex, thus making it hard to obtain the optimal solution of the GTRPCA model. In this paper, we design an efficient algorithm optimization framework based on half-quadratic theory (Nikolova and Ng 2005) and ADMM framework (Boyd et al. 2011) to implement GTRPCA model.

Proposition 1. *For the proposed Generalized loss function $g(x)$, there exists a convex conjugate function $\psi : \mathbb{R} \rightarrow \mathbb{R}$ which satisfied*

$$g(x) = \min_{w \in \mathbb{R}_+} (w|x| + \psi(w)), \quad (9)$$

and for fixed x , the minimum is reached at $w = \xi(x)$, which is defined as

$$w = \xi(x) = \begin{cases} 1, & \text{if } \alpha = 2 \\ 2c/(|x| + 2c), & \text{if } \alpha = 0 \\ \exp(-|x|/2c), & \text{if } \alpha = -\infty \\ \left(\frac{|x|/c}{|\alpha-2|} + 1\right)^{\alpha/2-1}, & \text{otherwise.} \end{cases} \quad (10)$$

Remark 2. According to Proposition 1, the loss function in Eq. (6) can be optimized by an adaptive alternating weighted minimization scheme. From the perspective of weights, smaller weights represent smaller shrinkages to singular values. As shown in Fig. 3(b), TNN assigns the same weights to each singular value, i.e., TNN treats each singular value equally. For our proposed GTNN, large singular values will be adaptively assigned small weights and shrunk less. Meanwhile, it is evident that TNN is a special case of GTNN when $\alpha = 2$.

According to Proposition 1, GTNN can be transformed into

$$\|\mathcal{L}\|_{G,*} = \min_{\mathbf{W}} \frac{1}{d_3} \sum_{k=1}^{d_3} \sum_{i=1}^d (W_{ki} \sigma_i(\bar{\mathbf{L}}^{(k)}) + \psi(W_{ki})), \quad (11)$$

where the W_{ki} is the k, i -th element of matrix $\mathbf{W} \in \mathbb{R}^{d_3 \times d}$. The minimum is reached at $W_{ki} = \xi(\sigma_i(\bar{\mathbf{L}}^{(k)}); c^L)$. Similarly, as for GTL1N, we have

$$\|\mathcal{E}\|_{1,*} = \min_{\mathbf{W}} \sum_{i=1}^{d_1} \sum_{j=1}^{d_2} \sum_{k=1}^{d_3} (\mathcal{W}_{ijk} |\mathcal{E}_{ijk}| + \psi(\mathcal{W}_{ijk})), \quad (12)$$

where the \mathcal{W}_{ijk} is the i, j, k -th element of tensor $\mathbf{W} \in \mathbb{R}^{d_1 \times d_2 \times d_3}$. The minimum is reached at $\mathcal{W}_{ijk} = \xi(|\mathcal{E}_{ijk}|; c^E)$.

Notably, problem (8) will be transformed into weighted tensor nuclear norm minimization problem (11) and weighted tensor ℓ_1 norm minimization problem (12), we next present the definitions of two important concepts: Weighted tensor nuclear norm (WTNN) and weighted tensor ℓ_1 norm.

Definition 6. (Weighted Tensor Nuclear Norm, WTNN) (Wang et al. 2023b) For a tensor $\mathcal{X} \in \mathbb{R}^{d_1 \times d_2 \times d_3}$ and a weight matrix $\mathbf{W} \in \mathbb{R}^{d \times d_3}$, $d = \min(d_1, d_2)$, the WTNN of \mathcal{X} is defined as

$$\|\mathcal{X}\|_{\mathbf{W},*} = \frac{1}{d_3} \sum_{k=1}^{d_3} \sum_{i=1}^d W_{ik} \sigma_i(\bar{\mathbf{X}}^{(k)}). \quad (13)$$

Definition 7. (Weighted Tensor ℓ_1 Norm, WTLIN) (Wang et al. 2023b) For a tensor $\mathcal{X} \in \mathbb{R}^{d_1 \times d_2 \times d_3}$ and a weight tensor $\mathbf{W} \in \mathbb{R}^{d_1 \times d_2 \times d_3}$, the WTLIN of \mathcal{X} is defined as

$$\|\mathcal{X}\|_{\mathbf{W},*} = \sum_{i=1}^{d_1} \sum_{j=1}^{d_2} \sum_{k=1}^{d_3} |\mathcal{W}_{ijk} \mathcal{E}_{ijk}|. \quad (14)$$

By incorporating Eq. (11) and Eq. (12) into model (8), and according to the definition of WTNN and WTLIN, we have

$$\begin{aligned} \min_{\mathcal{L}, \mathcal{E}, \mathbf{W}, \mathbf{W}} & \|\mathcal{L}\|_{\mathbf{W},*} + \lambda \|\mathcal{E}\|_{\mathbf{W},*} + \Psi(\mathbf{W}) + \Psi(\mathbf{W}) \\ \text{s.t. } & \mathcal{M} = \mathcal{L} + \mathcal{E}, \end{aligned} \quad (15)$$

where $\Psi(\mathbf{W})$ and $\Psi(\mathbf{W})$ are defined such that $(\Psi(\mathbf{W}))_{ki} = \psi(W_{ki})$ and $(\Psi(\mathbf{W}))_{ijk} = \psi(\mathcal{W}_{ijk})$. And the model (15) is referred to as Generalized TRPCA (GTRPCA).

Optimization for GTRPCA

In this part, we devise an efficient ADMM-based optimization algorithm framework for GTRPCA. Notably, previous works use predefined and fixed weights to limit the shrinkage of large singular values. For comparison, GTRPCA views the weights as variables that are updated in the iterations. Moreover, the formula of the weights varies with the change of the continuous-valued parameter α . This characteristic enables our model to adapt flexibly to volatile scenarios. The augmented Lagrangian function of the GTRPCA model is

$$\begin{aligned} L(\mathcal{L}, \mathcal{E}, \mathbf{W}, \mathbf{W}, \mathcal{Z}, \mu) = & \|\mathcal{L}\|_{\mathbf{W},*} + \lambda \|\mathcal{E}\|_{\mathbf{W},*} + \Psi(\mathbf{W}) \\ & + \Psi(\mathbf{W}) + \frac{\mu}{2} \left\| \mathcal{L} + \mathcal{E} - \mathcal{M} + \frac{\mathcal{Z}}{\mu} \right\|_F^2 - \frac{\mu}{2} \|\mathcal{Z}/\mu\|_F^2, \end{aligned} \quad (16)$$

where $\mathcal{Z} \in \mathbb{R}^{d_1 \times d_2 \times d_3}$ denotes the Lagrangian multiplier and μ is a positive parameter. Each variable can be updated alternately in the scheme of the ADMM framework.

Step1: Update \mathcal{L} by fixing the other variables:

$$\mathcal{L}_{t+1} = \arg \min_{\mathcal{L}} \frac{1}{\mu_t} \|\mathcal{L}\|_{\mathbf{W},*} + \frac{1}{2} \|\mathcal{L} - (\mathcal{M} - \mathcal{E}_t - \mathcal{Z}_t/\mu_t)\|_F^2. \quad (17)$$

The closed-form solution of (17) can be easily obtained with the following proximity operator.

Lemma 1. Given $\mathcal{X} \in \mathbb{R}^{d_1 \times d_2 \times d_3}$ with t-SVD $\mathcal{X} = \mathcal{U} * \mathcal{S} * \mathcal{V}^*$ and a weight matrix $\mathbf{W} \in \mathbb{R}^{d \times d_3}$, where \mathbf{w}_k is the k -th column of \mathbf{W} and $d = \min\{d_1, d_2\}$. Considering the following Weighted Tensor Nuclear Norm minimization (WTNNM) problem

$$\text{Prox}_{\|\cdot\|_{\mathbf{W},*}}(\mathcal{X}) = \arg \min_{\mathcal{L}} \|\mathcal{L} - \mathcal{X}\|_F^2 + \|\mathcal{L}\|_{\mathbf{W},*}, \quad (18)$$

where $\|\cdot\|_{\mathbf{W},*}$ denotes the WTNN, and $\text{Prox}_{\|\cdot\|_{\mathbf{W},*}}$ is defined as a proximal operator. For non-descending weights $0 \leq W_{1k} \leq W_{2k} \leq \dots \leq W_{dk}$ ($k = 1, \dots, d_3$), the problem (18) has the global solution which is defined as

$$\mathcal{L}^* = \text{Prox}_{\|\cdot\|_{\mathbf{W},*}}(\mathcal{X}) = \mathcal{U} * \text{ifft}(\mathcal{P}_{\mathbf{W}}(\bar{\mathcal{S}}), [], 3) * \mathcal{V}^*, \quad (19)$$

where $\mathcal{P}_{\mathbf{W}}(\bar{\mathcal{S}})$ is a tensor to meet the conditions of its k -th frontal slice is $\mathbf{P}_{\mathbf{w}_k}(\bar{\mathbf{S}}^{(k)})$ for $k = 1, \dots, d_3$. $\bar{\mathbf{S}}^{(k)}$ is the k -th frontal slice of $\bar{\mathcal{S}}$, and $\mathbf{P}_{\mathbf{w}_k}(\bar{\mathbf{S}}^{(k)})$ denotes a diagonal matrix which can be computed as $(\mathbf{P}_{\mathbf{w}_k}(\bar{\mathbf{S}}^{(k)}))_{ii} = (\bar{\mathbf{S}}_{ii}^{(k)} - w_{ki})_+$, where $(x)_+ = x$ if $x > 0$ and $(x)_+ = 0$ otherwise. w_{ki} is the i -th element of the \mathbf{w}_k .

By recalling the definition of WTNN in Definition 6, we have $\frac{1}{\mu_t} \|\mathcal{L}\|_{\mathbf{W},*} = \|\mathcal{L}\|_{\frac{1}{\mu_t} \mathbf{W},*}$. Based on Lemma 1, the solution of the subproblem (17) can be described as

$$\mathcal{L}_{t+1} = \text{Prox}_{\|\cdot\|_{\frac{1}{\mu_t} \mathbf{W},*}}(\mathcal{M} - \mathcal{E}_t - \mathcal{Z}_t / \mu_t). \quad (20)$$

Step2: Update \mathcal{E} by fixing other variables:

$$\mathcal{E}_{t+1} = \arg \min_{\mathcal{E}} \frac{\lambda}{\mu_t} \|\mathcal{E}\|_{\mathbf{W},1} + \frac{1}{2} \|\mathcal{E} - (\mathcal{M} - \mathcal{L}_t - \mathcal{Z}_t / \mu_t)\|_F^2. \quad (21)$$

To get the closed-form solution of the above problem, we utilize the tensor soft-thresholding operator (TST) defined below to update \mathcal{E}_{t+1} .

$$\mathcal{E}_{t+1} = \text{TST}(\mathcal{M} - \mathcal{L}_t - \mathcal{Z}_t / \mu_t, \frac{\lambda}{\mu_t} \mathbf{W}_t), \quad (22)$$

where the ijk -th entry of TST is defined by

$$(\text{TST}(\mathcal{X}, \mathbf{W}))_{ijk} = \text{sign}(\mathcal{X}_{ijk})(|\mathcal{X}_{ijk}| - \mathbf{W}_{ijk})_+. \quad (23)$$

Step3: Update the elements of \mathbf{W} and \mathbf{W} by an adaptive way according to Proposition 1

$$W_{ki} = \xi(\sigma_i(\bar{\mathbf{L}}_{t+1}^{(k)}; c^L), \mathbf{W}_{ijk} = \xi(|(\mathcal{E}_{t+1})_{ijk}|; c^E)). \quad (24)$$

Step4: Update the Lagrangian multiplier tensor \mathcal{Z} and the parameter μ by

$$\mathcal{Z}_{t+1} = \mathcal{Z}_t + \mu_t(\mathcal{L}_{t+1} + \mathcal{E}_{t+1} - \mathcal{M}), \quad (25)$$

$$\mu_{t+1} = \rho \mu_t, \quad (26)$$

where $\rho = 1.1$, usually. The whole optimization procedure is summarized in Algorithm 1.

Algorithm 1: GTRPCA

Input: Observation tensor data $\mathcal{M} \in \mathbb{R}^{d_1 \times d_2 \times d_3}$, and the parameter λ .

Initialization: $\mathcal{L}_0 = \mathcal{E}_0 = \mathcal{Z}_0 = 0$, $\mathbf{W}_0 = \mathbf{1}_{d_3 \times d}$, $\mathbf{W}_0 = \mathbf{1}_{d_1 \times d_2 \times d_3}$, $\mu_0 = 10^{-2}$, $\rho = 1.1$, $\epsilon = 10^{-6}$, and $t = 0$.

- 1: **while** not converge **do**
- 2: Update the low-rank tensor \mathcal{L} by Eq. (17).
- 3: Update the sparse tensor \mathcal{E} by Eq. (21).
- 4: Update the weights \mathbf{W} and \mathbf{W} by Eq. (24).
- 5: Update the Lagrangian multiplier \mathcal{Z} by Eq. (25).
- 6: Update the parameter μ by Eq. (26).
- 7: Check the convergence condition:

$$\|\mathcal{L}_{t+1} - \mathcal{L}_t\|_\infty < \epsilon, \|\mathcal{E}_{t+1} - \mathcal{E}_t\|_\infty < \epsilon,$$

$$\|\mathcal{M} - \mathcal{L}_{t+1} - \mathcal{E}_{t+1}\|_\infty < \epsilon.$$
- 8: **end while**

Output: $\mathcal{L} = \mathcal{L}_{t+1}, \mathcal{E} = \mathcal{E}_{t+1}$

Smooth FGTRPCA

Considering a structured tensor that exhibits both global low-rankness and local smoothness, existing approaches typically represent these properties as the sum of two separate prior terms. This separation leads to the challenge of balancing the two regularizers. However, recent research suggests that incorporating the low-rank structure of gradient tensors can create a joint prior, effectively capturing both global low-rankness and local smoothness structures. Before proceeding with further discussion, we introduce the definition of the gradient tensor as follows, with Γ representing the set of all directions considered a priori.

Definition 8. (*Gradient tensor*) (Wang et al. 2023a) For a tensor $\mathcal{X} \in \mathbb{R}^{d_1 \times d_2 \times d_3}$, its gradient tensor along the k -th mode is defined as

$$\mathcal{G}_k := \nabla_k(\mathcal{X}) = \mathcal{X} \times_k \mathbf{D}_{n_k}, k = 1, 2, 3, \quad (27)$$

where \mathbf{D}_{n_k} is a row circulant matrix of $(-1, 1, 0, \dots, 0)$.

As widely recognized, evaluating the gradient tensor using a specific norm called total variation (TV) has become a pivotal method for representing local smoothness, e.g., $\|\mathcal{X}\|_{\text{TV}} := \sum_{k \in \Gamma} \|\mathcal{G}_k\|_1$. In recent works, (Wang et al. 2023a) proposed tensor correlated total variation (t-CTV) norm to encode the two priors simultaneously with exact recoverability guarantees in theory. However, the regularizer is modeled by TNN in the gradient domain, which confronts the same obstacle corresponding to TRPCA. Fortunately, our proposed FGTRPCA can similarly model the gradient tensors to improve the performance. Consequently, we propose a novel tensor-correlated Flexible Generalized Joint Prior (t-FGJP) regularizer that better approximates the low-rank component. The definition of t-FGJP is as follows.

Definition 9. (*t-FGJP*) For a tensor $\mathcal{X} \in \mathbb{R}^{d_1 \times d_2 \times d_3}$, the proposed t-FGJP norm is defined as

$$\|\mathcal{X}\|_{\text{t-FGJP}} := \frac{1}{\gamma} \sum_{k \in \Gamma} \|\mathcal{G}_k\|_{G,*,\mathfrak{L}}, \quad (28)$$

where Γ represents a priori set of directions along which \mathcal{X} equips both global low-rankness and local smoothness priors and $\gamma := \#\{\Gamma\}$ denotes the cardinality of Γ . By incorporating both t-FGJP and FGTL1N into the TRPCA framework, we propose a smooth FGTRPCA (SFGTRPCA) model defined as

$$\min_{\mathcal{L}, \mathcal{E}} \|\mathcal{L}\|_{t\text{-FGJP}} + \lambda \|\mathcal{E}\|_{G,1} \text{ s.t. } \mathcal{M} = \mathcal{L} + \mathcal{E}. \quad (29)$$

The SGTRPCA optimization problem is similar to the GTRPCA problem. Details of the optimization algorithm and the entire procedure are available in the supplementary material due to space limitations.

Experiments

To substantiate the effectiveness of the proposed methods, we present several real-world experiments involving denoising tasks applied to various tensor data types to evaluate the performance of our models.

Settings

Databases: We use 4 widely used tensor data types including color images, grayscale videos, hyperspectral images (HSIs), and multispectral images (MSIs). For color images, we choose 3 widely used datasets including Berkeley Segmentation Dataset¹ (BSD) (Martin et al. 2001), Kodak (Kodak 1993) dataset², and ZheJiang University (ZJU) (Hu et al. 2012) dataset³. For grayscale videos, we 14 grayscale video sequences from the YUV database⁴ and select the first 100 frames for each sequence, resulting in fourteen $144 \times 176 \times 100$ tensors. For HSIs, we select Cuprite⁵, DCMall⁶, Urban⁷, Indian Pines⁸, and Pavia University⁹ (PaviaU) for experiments. After selecting the first 50 bands from each HSI database, all HSIs used in the experiments were pre-processed to a size of $256 \times 190 \times 50$, $200 \times 200 \times 50$, $256 \times 190 \times 50$, $307 \times 307 \times 50$, $145 \times 145 \times 50$, and $610 \times 340 \times 50$, respectively. For MSIs, we randomly select 10 MSIs from the CAVE database (Yasuma et al. 2008) with the size of $256 \times 256 \times 31$.

Baselines: Our baselines for comparison are TRPCA (Lu et al. 2020), t-CTV (Wang et al. 2023a), and RTCTV (Huang et al. 2024).

Evaluation metrics: The peak signal-to-noise ratio (PSNR), structural similarity (SSIM), and feature similarity (FSIM) are employed to evaluate the recovery performance for color images and grayscale videos. For HSIs and MSIs, we adopt the PSNR, SSIM, and Erreur Relative Globale Adimensionnelle de Synthese (ERGAS) for evaluation.

¹<https://www2.eecs.berkeley.edu/Research/Projects/CS/vision/bsds/>

²<http://r0k.us/graphics/kodak/>

³<https://sites.google.com/site/zjuyaohu/>

⁴<http://trace.eas.asu.edu/yuv/>

⁵<https://lesun.weebly.com/hyperspectral-data-set.html>

⁶<https://lesun.weebly.com/hyperspectral-data-set.html>

⁷<https://lesun.weebly.com/hyperspectral-data-set.html>

⁸<https://lesun.weebly.com/hyperspectral-data-set.html>

⁹<https://lesun.weebly.com/hyperspectral-data-set.html>

Parameter settings: For fair comparison, the regularization parameter λ is set to $1/\sqrt{3\max(d_1, d_2)}$ for all methods. Specifically, for the parameter α in our models, we search from a candidate set and employ the parameter that demonstrates optimal performance in most cases ($\alpha = 1$).

Noise settings: For each channel of the color image, each frame of the grayscale video, and each band of HSI and MSI, we introduce random salt and pepper noise at varying noise ratios of 10%, 20%, and 30%.

Results

Visual Quality. To clearly illustrate the advantages of our method, Fig. 4 presents several sample images from the BSD dataset, along with the recovery results under 20% salt and pepper noise. The PSNR and SSIM values are listed above the recovered images to enhance the credibility of the results. From the results, it is evident that SGTRPCA constructs more image details and color information (Especially the contour and color of the moon in the 3rd image). In the other hand, we have observed that the proposed GTRPCA and SGTRPCA methods significantly enhance the baseline methods (TRPCA and t-CTV) under both priors. This improvement is attributed to our newly proposed regularization terms, which better preserve critical information of low-rank and sparse components.

Quantitative Quality. In terms of quantitative quality, numerical results generated from all the competitors are presented in Tables 3, 5, 4, and 6 on color images, grayscale videos, HSIs, and MSIs. From the results, we make the following conclusions:

- Firstly, our proposed GTRPCA outperforms the baseline TRPCA algorithm. This is because of the ability of our proposed regularizer to assign large penalties to small singular values of the low-rank component and small entries of the sparse component compared to TNN. This strategy better preserves critical information and achieves better recovery performance. Moreover, by integrating the local smoothness prior, SGTRPCA obtains performance improvement over GTRPCA and outperforms the competitive methods. This is due to the fact that our regularizer can analogously enhance the performance of TNN in the gradient domain.
- Secondly, It is evident that under varying noise levels in different data types, SGTRPCA consistently yields competitive scores of evaluation indices. This demonstrates that our method better leverages the underlying low-rank and sparse structures within the tensor, exhibiting strong recovery ability and robustness. For instance in the BSD color image dataset, with the noise ratio to 10.81%, SGTRPCA averagely achieves 10.81% improvement compared to the second-best algorithm.

Conclusion

In this paper, we consider the Tensor RPCA problem, which aims to recover low-rank and sparse components from observed data. We propose a generalized and flexible low-rank regularization term to preserve critical information in the

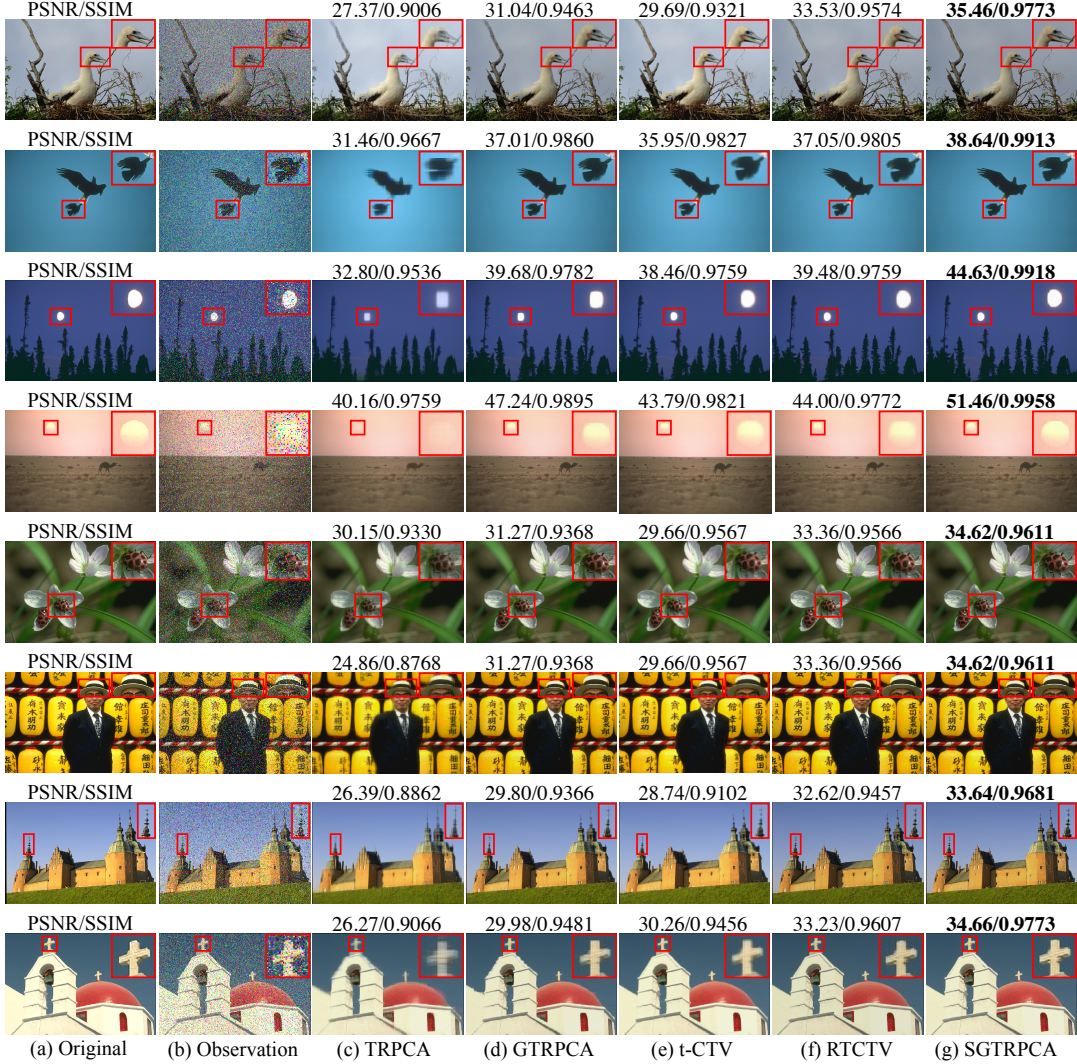


Figure 4: Recovery results for multiple color images from the BSD dataset.

Database	Noise Ratio	10%			20%			30%		
		Methods	PSNR	SSIM	FSIM	PSNR	SSIM	FSIM	PSNR	SSIM
BSD	TRPCA	29.62	0.9385	0.9467	27.95	0.8979	0.9227	26.30	0.8273	0.8907
	GTRPCA	35.79	0.9755	0.9845	31.92	0.9387	0.9460	28.90	0.8626	0.9286
	t-CTV	31.29	0.9442	0.9604	30.16	0.9232	0.9472	29.05	0.8955	0.9307
	SGTRPCA	39.66	0.9896	0.9937	35.39	0.9720	0.9836	32.42	0.9410	0.9671
Kodak	TRPCA	29.63	0.9323	0.9651	28.26	0.8946	0.9517	26.89	0.8317	0.9334
	GTRPCA	35.74	0.9744	0.9929	32.23	0.9143	0.9822	29.10	0.8873	0.9662
	t-CTV	31.69	0.9412	0.9847	30.69	0.9209	0.9792	29.71	0.8946	0.9715
	SGTRPCA	37.64	0.9793	0.9958	35.00	0.9590	0.9914	32.71	0.9387	0.9854
ZJU	TRPCA	34.37	0.9685	0.9730	32.44	0.9419	0.9576	30.27	0.8812	0.9339
	GTRPCA	40.26	0.9889	0.9927	35.64	0.9714	0.9804	33.35	0.9423	0.9647
	t-CTV	35.54	0.9722	0.9807	34.27	0.9603	0.9729	32.86	0.9426	0.9621
	SGTRPCA	43.88	0.9946	0.9966	39.38	0.9865	0.9913	36.42	0.9714	0.9825

Table 3: Quantitative comparisons of color image completion results with different noise ratios.

Database	Noise Ratio	10%			20%			30%		
		Methods	PSNR	SSIM	ERGAS	PSNR	SSIM	ERGAS	PSNR	SSIM
Cuprite	TRPCA	54.85	0.9948	23.29	52.07	0.9937	25.26	48.96	0.9918	27.46
	GTRPCA	59.56	0.9976	11.59	56.46	0.9967	13.33	52.94	0.9953	15.75
	t-CTV	56.72	0.9961	17.29	54.85	0.9956	18.39	52.68	0.9947	19.43
	SGTRPCA	62.68	0.9983	10.02	60.38	0.9976	12.93	58.47	0.9971	13.63
DC Mall	TRPCA	44.96	0.9834	65.25	42.81	0.9811	70.76	39.95	0.9775	78.02
	GTRPCA	47.92	0.9933	34.19	44.74	0.9873	49.85	41.55	0.9827	61.72
	t-CTV	46.68	0.9887	46.53	44.55	0.9873	49.93	42.12	0.9854	54.14
	SGTRPCA	54.54	0.9953	29.32	51.78	0.9938	34.06	46.22	0.9914	39.17
Urban	TRPCA	46.98	0.9951	34.47	45.29	0.9937	38.73	43.12	0.9907	44.85
	GTRPCA	49.60	0.9972	21.71	47.16	0.9952	29.12	44.76	0.9923	36.58
	t-CTV	48.94	0.9964	25.64	47.56	0.9956	28.13	45.96	0.9944	31.54
	SGTRPCA	58.87	0.9989	12.29	55.40	0.9983	14.62	53.20	0.9972	19.94
Indain Pines	TRPCA	35.55	0.9320	69.89	34.68	0.9229	72.58	33.27	0.8976	77.94
	GTRPCA	38.77	0.9587	51.10	37.03	0.9443	57.38	35.51	0.9279	64.26
	t-CTV	36.50	0.9356	64.96	35.98	0.9312	66.30	35.30	0.9245	68.41
	SGTRPCA	40.43	0.9640	47.74	39.00	0.9553	50.95	37.15	0.9419	57.34
PaviaU	TRPCA	38.59	0.9718	63.04	37.55	0.9677	68.64	36.45	0.9619	75.46
	GTRPCA	40.69	0.9825	47.60	39.13	0.9703	56.53	37.68	0.9622	66.33
	t-CTV	39.80	0.9729	55.42	39.03	0.9702	59.03	38.25	0.9668	63.04
	SGTRPCA	45.42	0.9876	34.47	44.28	0.9834	37.32	42.18	0.9767	44.26

Table 4: Quantitative comparisons of HSIs completion results with different noise ratios.

low-rank components. A key advantage of our approach is the introduction of a continuous parameter α , which allows us to adjust the form of the proposed regularization term to enhance performance. Furthermore, we extend the proposed regularization term to the sparse components, leading to the GTRPCA model. We have shown that some existing models are special cases of our proposed model. Beyond the inherent global low-rankness structure of natural tensors, some tensor data also exhibits local smoothness structures. Fortunately, our proposed low-rank regularization term integrates well with the t-CTV model, prompting the introduction of the SGTRPCA model. Experimental results demonstrate that our models significantly improve the benchmark performance on tensor denoising tasks.

References

- Boyd, S.; Parikh, N.; Chu, E.; Peleato, B.; Eckstein, J.; et al. 2011. Distributed optimization and statistical learning via the alternating direction method of multipliers. *Foundations and Trends® in Machine learning*, 3(1): 1–122.
- Gao, Q.; Zhang, P.; Xia, W.; Xie, D.; Gao, X.; and Tao, D. 2020. Enhanced tensor RPCA and its application. *IEEE transactions on pattern analysis and machine intelligence*, 43(6): 2133–2140.
- Hitchcock, F. L. 1927. The expression of a tensor or a polyadic as a sum of products. *Journal of Mathematics and Physics*, 6(1-4): 164–189.
- Hou, J.; Liu, X.; Wang, H.; and Guo, K. 2024. Tensor recovery from binary measurements fused low-rankness and smoothness. *Signal Processing*, 221: 109480.
- Hu, Y.; Zhang, D.; Ye, J.; Li, X.; and He, X. 2012. Fast and accurate matrix completion via truncated nuclear norm regularization. *IEEE transactions on pattern analysis and machine intelligence*, 34(3): 549–560.
- Kilmer, M.; Braman, K.; Hao, N.; and Hoover, R. C. 2013. Third-order tensors as operators on matrices: A theoretical and computational framework with applications in imaging. *SIAM J. Matrix Anal. Appl.*, 34(1): 148–172.
- Kilmer, M.; and Martin, C. 2011. Factorization strategies for third-order tensors. *Linear Algebra Appl.*, 435(3): 641–658.
- Kilmer, M. E.; Horesh, L.; Avron, H.; and Newman, E. 2021. Tensor-tensor algebra for optimal representation and compression of multiway data. *Proceedings of the National Academy of Sciences*, 118(28): e2015851118.
- Ko, C.-Y.; Batselier, K.; Daniel, L.; Yu, W.; and Wong, N. 2020. Fast and accurate tensor completion with total variation regularized tensor trains. *IEEE Transactions on Image Processing*, 29: 6918–6931.
- Kodak. 1993. Kodak lossless true color image suite (PhotoCD PCD0992). URL <http://r0k.us/graphics/kodak>, 6: 2.

- Kolda, T. G.; and Bader, B. W. 2009. Tensor decompositions and applications. *SIAM review*, 51(3): 455–500.
- Liu, Y.; Du, B.; Chen, Y.; Zhang, L.; Gong, M.; and Tao, D. 2024a. Convex–Concave Tensor Robust Principal Component Analysis. *International Journal of Computer Vision*, 132(5): 1721–1747.
- Liu, Y.; Wang, Y.; Chen, L.; Wang, L.; and Hu, Y. 2024b. TIHN: Tensor Improved Huber Norm for Low-rank Tensor Recovery. *International Journal of Wavelets, Multiresolution and Information Processing*.
- Liu, Z.; Han, Z.; Tang, Y.; Zhao, X.-L.; and Wang, Y. 2024c. Low-Tubal-Rank Tensor Recovery via Factorized Gradient Descent. *arXiv preprint arXiv:2401.11940*.
- Lu, C.; Feng, J.; Chen, Y.; Liu, W.; Lin, Z.; and Yan, S. 2020. Tensor Robust Principal Component Analysis with a New Tensor Nuclear Norm. *IEEE Trans. Pattern Anal. Mach. Intell.*, 42(4): 925–938.
- Martin, D.; Fowlkes, C.; Tal, D.; and Malik, J. 2001. A database of human segmented natural images and its application to evaluating segmentation algorithms and measuring ecological statistics. In *Proceedings eighth IEEE international conference on computer vision. ICCV 2001*, volume 2, 416–423. IEEE.
- Nikolova, M.; and Ng, M. K. 2005. Analysis of half-quadratic minimization methods for signal and image recovery. *SIAM Journal on Scientific computing*, 27(3): 937–966.
- Peng, J.; Wang, H.; Cao, X.; Liu, X.; Rui, X.; and Meng, D. 2022. Fast noise removal in hyperspectral images via representative coefficient total variation. *IEEE Transactions on Geoscience and Remote Sensing*, 60: 1–17.
- Peng, J.; Xie, Q.; Zhao, Q.; Wang, Y.; Yee, L.; and Meng, D. 2020. Enhanced 3DTV regularization and its applications on HSI denoising and compressed sensing. *IEEE Transactions on Image Processing*, 29: 7889–7903.
- Phothilimthana, M.; Abu-El-Haija, S.; Cao, K.; Fatemi, B.; Burrows, M.; Mendis, C.; and Perozzi, B. 2024. Tpugraphs: A performance prediction dataset on large tensor computational graphs. *Advances in Neural Information Processing Systems*, 36.
- Qin, W.; Wang, H.; Zhang, F.; Ma, W.; Wang, J.; and Huang, T. 2024. Nonconvex Robust High-Order Tensor Completion Using Randomized Low-Rank Approximation. *IEEE Transactions on Image Processing*.
- Qiu, D.; Bai, M.; Ng, M. K.; and Zhang, X. 2021. Robust low-rank tensor completion via transformed tensor nuclear norm with total variation regularization. *Neurocomputing*, 435: 197–215.
- Wang, H.; Peng, J.; Qin, W.; Wang, J.; and Meng, D. 2023a. Guaranteed tensor recovery fused low-rankness and smoothness. *IEEE Transactions on Pattern Analysis and Machine Intelligence*, 45(9): 10990–11007.
- Wang, Y.; Kou, K. I.; Chen, H.; Tang, Y. Y.; and Li, L. 2023b. Double Auto-Weighted Tensor Robust Principal Component Analysis. *IEEE Transactions on Image Processing*.
- Wen, T.; Chen, E.; and Chen, Y. 2024. Tensor-view topological graph neural network. In *International Conference on Artificial Intelligence and Statistics*, 4330–4338. PMLR.
- Yan, T.; and Guo, Q. 2024. Tensor robust principal component analysis via dual lp quasi-norm sparse constraints. *Digital Signal Processing*, 150: 104520.
- Yasuma, F.; Mitsunaga, T.; Iso, D.; and Nayar, S. K. 2008. Generalized Assorted Pixel Camera: Post-Capture Control of. *Tech. rep., Department of Computer Science, Columbia University CUCS-061-08*.
- Zhang, C.; Li, H.; Lv, W.; Huang, Z.; Gao, Y.; and Chen, C. 2023a. Enhanced tensor low-rank and sparse representation recovery for incomplete multi-view clustering. In *Proceedings of the AAAI conference on artificial intelligence*, volume 37, 11174–11182.
- Zhang, F.; Wang, H.; Qin, W.; Zhao, X.; and Wang, J. 2023b. Generalized nonconvex regularization for tensor RPCA and its applications in visual inpainting. *Applied Intelligence*, 53(20): 23124–23146.
- Zhao, L.; Xu, X.; Wang, Z.; Zhang, Y.; Zhang, B.; Zheng, W.; Du, D.; Zhou, J.; and Lu, J. 2024. LowRankOcc: Tensor Decomposition and Low-Rank Recovery for Vision-based 3D Semantic Occupancy Prediction. In *Proceedings of the IEEE/CVF Conference on Computer Vision and Pattern Recognition*, 9806–9815.

Database	Noise Ratio	10%			20%			30%		
		Methods	PSNR	SSIM	FSIM	PSNR	SSIM	FSIM	PSNR	SSIM
Akiyo	TRPCA	38.03	0.9859	0.9897	37.00	0.9826	0.9875	35.90	0.9784	0.9846
	GTRPCA	46.25	0.9968	0.9974	43.79	0.9949	0.9960	41.08	0.9921	0.9940
	t-CTV	40.77	0.9912	0.9938	39.84	0.9896	0.9927	38.73	0.9874	0.9911
	SGTRPCA	50.92	0.9982	0.9987	48.00	0.9970	0.9980	45.54	0.9957	0.9971
Carphone	TRPCA	32.58	0.9549	0.9655	31.86	0.9454	0.9599	31.02	0.9283	0.9516
	GTRPCA	37.52	0.9760	0.9856	35.17	0.9521	0.9739	33.65	0.9424	0.9669
	t-CTV	34.33	0.9658	0.9739	33.75	0.9610	0.9707	33.17	0.9551	0.9669
	SGTRPCA	39.79	0.9864	0.9913	37.78	0.9782	0.9862	36.22	0.9675	0.9798
Claire	TRPCA	39.18	0.9878	0.9898	37.96	0.9848	0.9873	36.94	0.9811	0.9844
	GTRPCA	48.48	0.9964	0.9975	45.01	0.9943	0.9959	42.59	0.9905	0.9937
	t-CTV	41.78	0.9920	0.9942	40.88	0.9907	0.9931	39.94	0.9890	0.9918
	SGTRPCA	51.31	0.9978	0.9986	47.99	0.9963	0.9977	45.73	0.9947	0.9966
Coastguard	TRPCA	30.56	0.9181	0.9377	29.44	0.8920	0.9260	27.99	0.8414	0.9091
	GTRPCA	35.67	0.9651	0.9769	32.77	0.9367	0.9612	30.59	0.9026	0.9422
	t-CTV	31.34	0.9227	0.9465	30.53	0.9070	0.9381	29.74	0.8875	0.9290
	SGTRPCA	36.77	0.9749	0.9835	34.13	0.9545	0.9723	32.13	0.9332	0.9579
Container	TRPCA	41.71	0.9913	0.9937	40.34	0.9888	0.9923	38.20	0.9839	0.9900
	GTRPCA	49.40	0.9961	0.9975	46.69	0.9942	0.9964	44.54	0.9907	0.9951
	t-CTV	43.94	0.9931	0.9956	42.41	0.9915	0.9948	40.81	0.9891	0.9936
	SGTRPCA	52.08	0.9977	0.9986	49.71	0.9966	0.9980	46.97	0.9951	0.9972
Foreman	TRPCA	31.65	0.9450	0.9504	30.36	0.9230	0.9370	28.93	0.8767	0.9164
	GTRPCA	38.42	0.9783	0.9854	35.03	0.9592	0.9720	32.20	0.9303	0.9523
	t-CTV	33.77	0.9606	0.9626	32.67	0.9497	0.9544	31.62	0.9345	0.9441
	SGTRPCA	41.23	0.9869	0.9915	37.97	0.9755	0.9831	35.26	0.9582	0.9702
Hall	TRPCA	34.00	0.9773	0.9802	33.32	0.9739	0.9781	32.53	0.9688	0.9753
	GTRPCA	39.88	0.9896	0.9933	37.78	0.9845	0.9902	35.97	0.9807	0.9851
	t-CTV	36.62	0.9838	0.9862	36.20	0.9822	0.9851	35.65	0.9802	0.9835
	SGTRPCA	42.05	0.9943	0.9954	40.39	0.9888	0.9929	39.09	0.9872	0.9910
Miss-america	TRPCA	38.64	0.9784	0.9792	37.54	0.9729	0.9746	36.35	0.9641	0.9683
	GTRPCA	46.49	0.9934	0.9952	43.49	0.9885	0.9916	41.01	0.9782	0.9856
	t-CTV	41.43	0.9851	0.9876	40.60	0.9826	0.9853	39.75	0.9794	0.9827
	SGTRPCA	49.20	0.9957	0.9973	46.57	0.9926	0.9953	44.52	0.9890	0.9929
Mobile	TRPCA	28.66	0.9472	0.9680	27.02	0.9205	0.9537	25.22	0.8668	0.9252
	GTRPCA	34.39	0.9760	0.9842	30.37	0.9551	0.9736	27.88	0.9123	0.9501
	t-CTV	29.59	0.9543	0.9745	28.18	0.9366	0.9652	26.78	0.9103	0.9512
	SGTRPCA	37.26	0.9871	0.9907	33.38	0.9737	0.9826	30.24	0.9463	0.9669
Mother-daughter	TRPCA	39.18	0.9729	0.9811	38.01	0.9667	0.9772	36.81	0.9576	0.9721
	GTRPCA	44.62	0.9898	0.9938	42.29	0.9840	0.9903	40.28	0.9769	0.9859
	t-CTV	41.25	0.9795	0.9867	40.37	0.9762	0.9847	39.43	0.9717	0.9819
	SGTRPCA	47.52	0.9937	0.9966	45.23	0.9901	0.9946	43.50	0.9861	0.9922
News	TRPCA	33.70	0.9667	0.9760	32.97	0.9616	0.9726	32.16	0.9549	0.9681
	GTRPCA	40.15	0.9880	0.9923	38.03	0.9834	0.9892	35.87	0.9763	0.9843
	t-CTV	36.50	0.9802	0.9854	35.90	0.9775	0.9836	35.19	0.9740	0.9812
	SGTRPCA	42.83	0.9940	0.9956	41.19	0.9906	0.9938	39.17	0.9874	0.9914
Salesman	TRPCA	37.81	0.9761	0.9817	36.90	0.9718	0.9772	35.89	0.9662	0.9744
	GTRPCA	44.77	0.9934	0.9951	42.08	0.9891	0.9921	40.16	0.9841	0.9888
	t-CTV	40.06	0.9834	0.9875	39.29	0.9811	0.9858	38.48	0.9781	0.9835
	SGTRPCA	47.20	0.9955	0.9968	44.86	0.9931	0.9951	42.89	0.9902	0.9932
Silent	TRPCA	34.00	0.9658	0.9762	33.30	0.9603	0.9729	32.61	0.9528	0.9690
	GTRPCA	40.58	0.9892	0.9928	38.18	0.9787	0.9876	36.44	0.9721	0.9831
	t-CTV	36.81	0.9768	0.9833	36.29	0.9738	0.9816	35.80	0.9703	0.9795
	SGTRPCA	43.16	0.9937	0.9954	40.82	0.9879	0.9922	39.09	0.9841	0.9892
Suzie	TRPCA	33.03	0.9356	0.9521	32.25	0.9229	0.9453	31.35	0.8999	0.9358
	GTRPCA	38.66	0.9745	0.9843	35.95	0.9588	0.9740	34.38	0.9292	0.9598
	t-CTV	34.86	0.9481	0.9630	34.29	0.9411	0.9588	33.68	0.9325	0.9537
	SGTRPCA	40.78	0.9813	0.9813	38.40	0.9708	0.9821	36.89	0.9582	0.9742

Table 5: Quantitative comparisons of color image completion results with different noise ratios.

Database	Noise Ratio Methods	10%			20%			30%		
		PSNR	SSIM	ERGAS	PSNR	SSIM	ERGAS	PSNR	SSIM	ERGAS
Balloons	TRPCA	42.46	0.9952	36.51	41.38	0.9938	40.83	39.91	0.9914	46.76
	GTRPCA	51.75	0.9986	12.06	48.20	0.9967	17.56	45.67	0.9953	23.99
	t-CTV	48.40	0.9981	20.53	47.44	0.9977	22.56	46.29	0.9972	25.36
	SGTRPCA	60.91	0.9995	6.06	57.26	0.9991	7.98	53.51	0.9987	11.43
Beads	TRPCA	34.16	0.9788	102.24	32.38	0.9691	121.56	30.45	0.9438	147.31
	GTRPCA	39.74	0.9889	48.25	36.45	0.9779	69.76	33.29	0.9560	100.96
	t-CTV	37.25	0.9864	68.58	35.96	0.9824	77.49	34.59	0.9757	88.79
	SGTRPCA	46.96	0.9964	27.22	43.00	0.9899	37.16	39.51	0.9834	56.09
Cd	TRPCA	31.85	0.9861	143.64	31.02	0.9838	158.19	29.90	0.9803	180.99
	GTRPCA	40.72	0.9951	53.67	38.76	0.9875	65.74	36.34	0.9748	85.17
	t-CTV	37.64	0.9932	74.43	37.12	0.9922	78.64	36.56	0.9909	83.77
	SGTRPCA	44.26	0.9981	36.15	43.86	0.9928	36.47	41.35	0.9907	48.61
Chart	TRPCA	43.75	0.9928	47.54	41.93	0.9908	53.74	39.94	0.9874	61.15
	GTRPCA	51.62	0.9977	21.16	47.15	0.9961	29.09	43.82	0.9922	37.74
	t-CTV	48.52	0.9958	33.22	46.86	0.9950	35.69	44.89	0.9939	39.24
	SGTRPCA	60.30	0.9982	24.24	55.66	0.9973	26.25	52.04	0.9955	33.10
Clay	TRPCA	48.83	0.9973	32.69	47.46	0.9965	36.38	45.75	0.9952	42.60
	GTRPCA	59.46	0.9995	10.69	55.41	0.9990	16.92	52.53	0.9981	21.46
	t-CTV	55.01	0.9989	19.51	53.61	0.9986	21.58	52.02	0.9983	23.95
	SGTRPCA	66.38	0.9998	7.31	61.95	0.9995	10.67	58.36	0.9992	17.74
Cloth	TRPCA	44.19	0.9847	36.04	40.77	0.9788	43.32	36.75	0.9608	58.27
	GTRPCA	49.24	0.9924	21.88	43.74	0.9871	30.43	39.80	0.9766	43.28
	t-CTV	46.56	0.9876	30.28	43.46	0.9844	34.86	40.46	0.9785	41.86
	SGTRPCA	55.45	0.9931	21.50	50.27	0.9903	26.45	45.39	0.9860	31.24
Egyptian	TRPCA	44.53	0.9950	61.16	43.38	0.9936	66.67	41.78	0.9912	75.79
	GTRPCA	50.39	0.9985	25.06	48.56	0.9974	31.40	46.57	0.9950	38.61
	t-CTV	48.92	0.9974	36.12	47.93	0.9969	41.12	45.98	0.9960	46.79
	SGTRPCA	63.29	0.9994	11.67	58.52	0.9990	14.82	53.33	0.9980	19.27
Feathers	TRPCA	40.50	0.9872	68.71	39.08	0.9844	75.24	37.41	0.9794	84.53
	GTRPCA	47.34	0.9956	28.41	43.68	0.9908	37.09	41.32	0.9864	51.99
	t-CTV	45.19	0.9925	44.17	44.01	0.9914	47.60	42.50	0.9898	51.84
	SGTRPCA	55.31	0.9976	20.73	51.35	0.9958	29.09	47.43	0.9930	40.57
Flowers	TRPCA	45.27	0.9847	65.33	43.12	0.9810	74.58	40.83	0.9746	87.24
	GTRPCA	53.07	0.9958	23.40	48.37	0.9917	34.31	44.91	0.9848	48.24
	t-CTV	50.33	0.9918	40.48	48.56	0.9905	44.17	46.52	0.9883	49.16
	SGTRPCA	61.20	0.9968	22.58	55.41	0.9939	32.13	50.57	0.9913	35.07
Glass	TRPCA	45.20	0.9965	34.70	43.66	0.9957	38.27	42.13	0.9942	42.67
	GTRPCA	53.97	0.9986	16.55	50.21	0.9977	22.64	47.32	0.9961	27.62
	t-CTV	48.40	0.9969	29.18	47.15	0.9965	31.35	45.73	0.9958	34.40
	SGTRPCA	59.66	0.9989	13.91	56.22	0.9983	18.22	52.90	0.9976	24.81

Table 6: Quantitative comparisons of MSIs completion results with different noise ratios.